Two-view Epipole-based Guidance Control for Autonomous Unmanned Aerial Vehicles

W. Achicanoy[1], C. Sagüés[2], G. López-Nicolás[2] and C. Rodríguez[1]
[1]*Departamento de Ingeniería Mecánica, Universidad de los Andes, Bogotá, Colombia*
[2]*Departamento de Informática e Ingeniería de Sistemas, Instituto de Investigación en Ingeniería de Aragón, Universidad de Zaragoza, Maria de Luna 1, E-50018, Zaragoza, Spain*

Keywords: UAV Guidance, Epipolar Geometry, Nonlinear Engagement, Input-output Linearization, State Feedback.

Abstract: A visual control based on epipolar geometry is proposed to guide an autonomous unmanned aerial vehicle (UAV) to a target position. The interest of this contribution resides in a new controller that allows purely vision-based guidance reducing the dependence on the accuracy of the system's state estimation using sensors as Inertial Measurement Units (IMU) and Global Positioning Systems (GPS). A current view and a target view are defined by a camera on-board the vehicle and a camera located at the target's position, respectively. The epipolar coordinates from these views are used to design a nonlinear control based on input-output linearization of the nonlinear engagement rule that relates the cameras' positions in time. An integrator is included to force the outputs (epipolar coordinates) to follow an equilibrium point and a state feedback control law is proposed to stabilize the outcome of the linearized input-output mapping. Simulation experiments for guidance of an small autonomous UAV with a classical three-loop autopilot are presented.

1 INTRODUCTION

Unmanned Aerial vehicles (UAVs) are used in civilian and military applications developing tasks of surveillance and delivering cargo. Over the last decade, UAVs have proved to be efficient in several missions around the world, motivating the aircraft industry in improving their internal systems and their capabilities. For example, a vision system could enable UAVs tracking a large number of targets (Schneiderman, 2012). The UAVs' performance commonly depends on aerial and ground operation centres and human assistance, but autonomous operation is necessary for stand-alone missions, or when the communication links fail and the vehicle needs to switch to a safe flight mode. The accuracy of the UAVs' flight depends on the on-board sensors' capabilities and its control robustness; the navigation and guidance systems usually use Inertial Measurement Units (IMU) and Global Positioning Systems (GPS), to get information of the self-position and self-attitude; on the other hand, they use cameras, spectrometers, and radars, to retrieve the target's features, position and attitude.

Cameras have been used in a wide range of applications for control of aerial, terrestrial, and aquatic vehicles, and vision-based control has become a special branch of research. Most of the research on vision-based control for autonomous UAVs have used cameras' information, together with inertial and global positioning sensors, as inputs for filters or estimators. For example, a vision-based guidance based on trajectory optimization is proposed in (Watanabe et al., 2006) and the vision data is used for an EKF to estimate the target's position and velocity relative to the vehicle. They include a cost function that minimizes the acceleration effort the vehicle demands to accomplish with three independent missions: Target interception, obstacle avoidance, and formation flight. In (Ma et al., 2007) a guidance law for a small UAV is developed based on an adaptive filter that calculates the target's velocity over the image plane. The filter only uses the tracking information of the moving target and a control law regulates the vehicle's yaw rate at a constant altitude (no depth information is required).

From another point of view, visual-based control methods based on epipolar geometry and homography have been used for mobile robot navigation. (Mariottini et al., 2004) and (López-Nicolás et al., 2008) have developed two-view visual-control for nonholonomic robots by means of nonlinear con-

Achicanoy W., Sagüés C., López-Nicolás G. and Rodríguez C..
Two-view Epipole-based Guidance Control for Autonomous Unmanned Aerial Vehicles.
DOI: 10.5220/0004032402420248
In *Proceedings of the 9th International Conference on Informatics in Control, Automation and Robotics* (ICINCO-2012), pages 242-248
ISBN: 978-989-8565-22-8

trol and tracking of epipoles signals. In (López-Nicolás et al., 2010) both epipolar geometry and homography matrix are used to design separated controls that are switched using information of the degeneracy of the fundamental matrix. Epipole-based control is used at the initial stage of the navigation, whereas homography-based control is used at the end (short baseline). Homography has been used for UAV navigation in (Hu et al., 2007b), where a multi-view visual-based control, that uses quaternions and homography between pre-recorded satellite images and the vehicle's actual images, is proposed to track a desired trajectory over the earth. Given that the estimated position is up to scale and the depth is unknown, open problems in this approach are clarified in (Hu et al., 2007a). In (Kaiser et al., 2010) a multi-view visual-based estimator based on homography and GPS measurements is designed; using this information an autopilot commands the vehicle's control surfaces. This estimator deals with two main challenges: The continuous tracking of features, entering and leaving the vehicle's camera Field of View (FoV), and the GPS failures.

Given that the epipolar geometry has reported successful outcomes in mobile robots, in this paper we presented the development of a new controller based on epipolar geometry for the guidance of an autonomous UAVs with a single camera on-board is developed. The vehicle motion is assumed to be planar. Two views, the current view (vehicle's camera) and the target view (static camera at the target's position), are used to compute the epipoles and to steer the vehicle to a desired position. As in (Mariottini et al., 2004) and (López-Nicolás et al., 2008), input-output linearization (Khalil, 2002) is used, but on the cameras' nonlinear engagement rule. The linearized output is stabilized by an appropriated state feedback control law and the outputs (epipolar coordinates) are forced to follow an equilibrium point by means of an integrator, that eliminates the steady state error and improves the robustness of the closed-loop system. Both epipolar coordinates in the current and target views are independently chosen as outputs. To deal with the complexity of the aerial vehicle model, a classical three-loop autopilot (Zarchan, 2007) is used to command the vehicle. The controller reduces the complexity of the on-board electronics, and the fact that only epipolar estimation is required, makes it suitable for simple guidance applications. The paper is organized as follows: in section 2 the planar epipolar geometry is shown; in section 3 a state space representation of the nonlinear planar engagement rule is presented; in section 4 the control strategy is developed; and in section 5 results of the simulation experiments are analyzed.

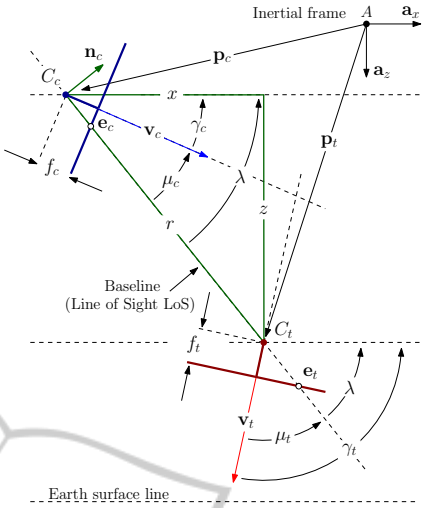

Figure 1: Planar two-view epipolar geometry (plane *xz*).

2 PLANAR EPIPOLAR GEOMETRY

Figure 1 shows the planar two-view epipolar geometry, relative to the inertial reference frame A, for the autonomous UAV guidance problem. The first view is defined by a current camera C_c on-board the vehicle, that is aligned with a current velocity vector $\mathbf{v}_c = [u_c^A, w_c^A]^T$ and is located at a current position $\mathbf{p}_c = [x_c^A, z_c^A]^T$, while the second view is an image previously defined by a target camera C_t, that is aligned with a target velocity $\mathbf{v}_t = [u_t^A, w_t^A]^T$ at a position $\mathbf{p}_t = [x_t^A, z_t^A]^T$. The epipoles $\mathbf{e}_c \in \mathbb{R}^2$ (current) and $\mathbf{e}_t \in \mathbb{R}^2$ (target) are subject to the constraints $F\mathbf{e}_c = \mathbf{0}$ and $F^T\mathbf{e}_t = \mathbf{0}$, where $F \in \mathbb{R}^{3\times3}$ is the fundamental matrix. F is estimated from a set of features correspondences using the RANSAC algorithm (Hartley and Zisserman, 2004). These epipoles can be written as $\mathbf{e}_c = [e_{c,w}, e_{c,h}]^T$ and $\mathbf{e}_t = [e_{t,w}, e_{t,h}]^T$, where $(e_{c,w}, e_{t,w})$ and $(e_{c,h}, e_{t,h})$ are the coordinates (in pixels) along the image's width and height, respectively. For planar guidance design, only the coordinates $(e_{c,h}, e_{t,h})$ are useful, and it follows that

$$e_{c,h} = f_c \tan(\lambda - \gamma_c) \tag{1a}$$

$$e_{t,h} = -f_t \tan(\gamma_t - \lambda), \tag{1b}$$

where f_c and f_t are the focal lengths for the current camera and the target camera, respectively; λ is the Line of Sight (LoS) angle, that is measured between the LoS and the $\mathbf{a}_x$-axis; and γ_c and γ_t are the flight path angles for the current camera and the target camera, respectively. These angles are measured between the velocity vectors ($\mathbf{v}_c$ and $\mathbf{v}_t$) and the $\mathbf{a}_x$-axis. By definition the baseline is equal to the LoS.

3 PLANAR ENGAGEMENT RULE

The planar engagement rule is a description of the evolution of the LoS angle λ and the LoS rate of change $\dot{\lambda}$ according to a lateral acceleration command $\mathbf{n}_c$. If $\mathbf{n}_c$ is proportional to $\dot{\lambda}$, then, the current camera C_c (vehicle) can be steered to the target camera C_t (target). This is the intuitive Proportional Navigation (PN) (Yanushevsky, 2007). From Fig. 1, $\lambda = \arctan(z/x)$, whit $x = x_t^A - x_c^A$ and $z = z_t^A - z_c^A$, and the LoS rate of change is

$$\dot{\lambda} = \frac{\dot{z}x - z\dot{x}}{r^2}\,, \tag{2}$$

where $r = \sqrt{x^2+z^2}$ is the magnitude of the instantaneous separation (range) between C_c and C_t. If (2) is differentiated again, taking into account that $\cos\lambda = x/r$ and $\sin\lambda = z/r$, it follows that

$$\ddot{\lambda} = \frac{\ddot{z}\cos\lambda - \ddot{x}\sin\lambda}{r} - \frac{2\dot{r}\dot{z}\cos\lambda + 2\dot{r}\dot{x}\sin\lambda}{r^2}\,. \tag{3}$$

Given that C_t is static, the C_c's acceleration components, in terms of the lateral acceleration magnitude n_c, are $\ddot{x} = -n_c\sin\lambda$ and $\ddot{z} = n_c\cos\lambda$, then, (3) can be symplified as

$$\ddot{\lambda} = \omega\sin(\lambda - \phi) + n_c/r\,, \tag{4}$$

where $\omega = 2(v_{cl}/r)^2$ and $\phi = \arctan(\dot{z}/\dot{x})$. $\mathbf{v}_{cl} = -\dot{\mathbf{r}}$ is commonly known as the closing velocity. Finally, the planar engagement can be presented as the continuous nonlinear system

$$\dot{\eta} = f(\eta, u) = \begin{bmatrix} \eta_2 \\ \omega\sin(\eta_1 - \phi) + u/r \end{bmatrix}\,, \tag{5}$$

where $\eta = [\eta_1, \eta_2]^T = [\lambda, \dot{\lambda}]^T \in \mathbb{R}^2$ is the state vector, $u = n_c \in \mathbb{R}$ is the input, and $f(\eta, u) : \mathbb{R}^2 \times \mathbb{R} \to \mathbb{R}^2$ is a vector field.

4 EPIPOLE-BASED GUIDANCE CONTROL

In this section, a guidance control based on input-output linearization of the engagement system (5) is presented. The output is based on the epipolar coordinates' measurements from the two images. The control law has the form of state feedback with integral action. Both, the coordinate $e_{c,h}$, defined by the Eq. (1a), and the coordinate $e_{t,h}$, defined by the Eq. (1b), can be independently used as outputs, i.e., $y = e_{c,h}$ or $y = e_{t,h}$. If y is differentiated until the input u becomes explicit it results that the relative degree of the system (5) is 2, for all $\eta \in \mathbb{R}^2$. We also obtain that either

$$\begin{aligned} u = \; & -r\omega\sin(\eta_1 - \phi) - 2r(\eta_2 - \dot{\gamma}_c)^2\tan(\eta_1 - \gamma_c) \\ & + r\ddot{\gamma}_c + \left[r\cos(\eta_1 - \gamma_c)^2/f_c\right] v \end{aligned} \tag{6}$$

for $y = e_{c,h}$, or

$$\begin{aligned} u = \; & -r\omega\sin(\eta_1 - \phi) + 2r\eta_2^2\tan(\gamma_t - \eta_1) \\ & + \left[r\cos(\gamma_t - \eta_1)^2/f_t\right] v\,, \end{aligned} \tag{7}$$

for $y = e_{t,h}$, lead the nonlinear output to the linearized mapping

$$\begin{aligned} \dot{\xi}_1 &= \xi_2 \\ \dot{\xi}_2 &= v \\ \dot{\sigma} &= e\,, \end{aligned} \tag{8}$$

where $\xi_1 = y$, $\xi_2 = \dot{y}$, v is the new control, and $e = \xi_1 - \xi_1^r = y - y^r$ is the output error. An integral action was included in (8) forcing the output y to follow a reference $\xi_1^r = y^r$. It is easily verified that the augmented system (8) with realization

$$A_a = \begin{bmatrix} 0 & 1 & 0 \\ 0 & 0 & 0 \\ 1 & 0 & 0 \end{bmatrix} \quad B_a = \begin{bmatrix} 0 \\ 1 \\ 0 \end{bmatrix} \quad C_a = \begin{bmatrix} 1 & 0 & 0 \end{bmatrix} \tag{9}$$

has a controllable pair (A_a, B_a), and a state feedback control

$$v = -\mathbf{K}[\xi, \sigma]^T\,, \tag{10}$$

where $\mathbf{K} = [k_1, k_2, k_3]$, can stabilize it. $\mathbf{K}$ is chosen such that the matrix $(A_a - B_a\mathbf{K})$ is Hurwitz (pole placement) (Khalil, 2002) and local stability is guaranteed.

5 SIMULATION EXPERIMENTS AND ANALYSIS

Figure 2 shows the model of an UAV, without propulsion and with a camera on-board, used to evaluate the guidance control. For simplicity, a wing-body-tail configuration with a horizontal control surface (wing) and a stabilizing fixed surface (tail) was selected. Fast control is guaranteed by means of the wing's deflection angle δ, even though nonlinearities and rear stability interferences might appear (Chin, 1961). Given that the downrange is limited, the earth is assumed to be flat. Three reference frames are defined: (i) The

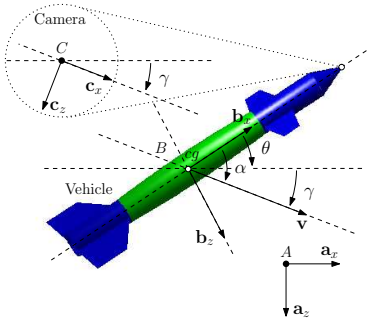

Figure 2: Autonomous UAV. The reference frames in the vertical plane *xz* are: *A* (inertial), *B* (vehicle-fixed), and *C* (camera-fixed).

inertial frame, named *A*, located at an initial altitude h_0; (ii) the vehicle-fixed frame, named *B*, aligned with the principal axes; and (iii) the camera-fixed frame, named *C*, aligned with the vehicle's velocity vector $\mathbf{v}$ or aero-stabilized. The camera's principal axis is parallel to the $\mathbf{c}_x$-axis and it is in the apex of the nose. The rotation and translation equations can be found in (Siouris, 2004). The estimation of the aerodynamic coefficients was computed using the Vortex Lattice Method (VLM) (Melin, 2000). For simplicity, the drag, lift and pitch coefficients depend only on the scheduling variables h (altitude) and M (Mach number) and are stored in look-up tables.

A classical three-loop autopilot (gyro and acceleration feedback), that translates acceleration commands u to wing deflections δ is also used. A complete description of the autopilot and the design equations can be found in (Zarchan, 2007). Fig. 3 shows the autopilot outputs for the step acceleration command $u = u_s(t-1)$ G (u_s is the unitary step function), for the flight conditions $h = 0$ m (black continuous lines), $h = 1000$ m (red dotted lines), $M = 0.3$, and $M = 0.9$. The actuator's dynamics are neglected and ideal sensors are assumed. The design parameters are $\omega_{CR} = 50$ rad/s (crossover frequency measured at the gain margin), $\zeta = 0.7$ (total acceleration damping), and $\tau = 0.2$ s (total acceleration time constant). Fig. 3(a) and Fig. 3(d) show the correspondence between the desired acceleration n and the autopilot's response for these parameters. It is noted that the vehicle's high manoeuvrability is reached at low altitude h and high Mach number M, and the angle of attack α and the deflection angle δ stay at low values (Fig. 3(e) and Fig. 3(f), respectively). For $M \leq 0.3$ the autopilot demands high values of α and δ (Fig. 3(b) and Fig. 3(c), respectively), and the vehicle's aerodynamic capabilities are exceeded. This flight condition can lead the system to instability. In order to deal with the change of the vehicle's parameters, according to the flight conditions, a look-up table (with linear interpolation) is implemented to select the autopilot gains according to the values of h and M.

On the other hand, it is assumed that the cameras C_c and C_t are identical, ideal (skew is zero), and with intrinsic parameters defined as in (Hartley and Zisserman, 2004). The image resolution is 480×640 pixels, the focal length is $f = f_c = f_t = 240$ pixel, and the epipoles' measurements are assumed to be known only from geometric relationships. For the simulations, the frame A is fixed at the initial altitude $h_0 = 2500$ m, the vehicle's initial velocity is $\mathbf{v}_0 = 200\mathbf{b}_x$ m/s, and the initial attitude angle θ is equal to the current camera C_c's attitude angle γ_c, i.e., the initial angle of attack $\alpha_0 = 0$ deg. The state feedback control gain $\mathbf{K}$ is calculated with the Acker's formula.

Initially, it is shown that the control with unforced output y, for both control laws (6) and (7) can be considered as PN-based control. This is explained by means of the differentiation of the Eq. (1b), that results in a directly proportional relationship between the rate of change of the target epipolar coordinate $\dot{e}_{t,h}$ and the LoS rate of change $\dot{\lambda}$. As in PN, the feedback of $\dot{e}_{t,h}$ multiplied by an appropriate constant can stabilize the linearized output (8), which means that the LoS angle λ is constant and the control based on $y = e_{t,h}$ can drive the vehicle to the target position (parallel navigation). An exact estimation of $\mathbf{v}_{cl}$ is not necessary. Furthermore, if the vehicle's path angle γ_c is replaced by a constant value, then, the differentiation of the Eq. (1a) results in a directly proportional relationship between $\dot{e}_{c,h}$ and $\dot{\lambda}$, and the control based on $y = e_{c,h}$ is able to drive the vehicle to the target position too. Fig. 4 shows the outputs of both control laws for three different initial current cameras $C_{c,1}$ at $\mathbf{p}_{c,1} = [0,0]^T$ m, $C_{c,2}$ at $\mathbf{p}_{c,2} = [500,0]^T$ m, and $C_{c,3}$ at $\mathbf{p}_{c,3} = [1000,0]^T$ m. The initial attitude angle is $\theta_0 = 45$ deg for all the cameras. Fig. 4(a) and Fig. 4(d) show that all cameras converge to the target camera C_t at $\mathbf{p}_t = [2000,2000]^T$ m ($\gamma_t = 90$ deg) for $y = e_{t,h}$ and $y = e_{c,h}$, respectively. The gain $\mathbf{K}$ is the same for both control laws and differences between them are mainly noted in the shape of the trajectories. Fig. 4(b) and Fig. 4(f) show that the epipolar coordinates $e_{t,h}$ and $e_{c,h}$ reach equilibrium points for both control laws. Fig. 4(c) and Fig. 4(e) show the free evolution of $e_{c,h}$ and $e_{t,h}$ for both control laws. The shape of the vehicle's trajectory is defined by the shape of the output epipolar coordinates. Fig. 5(a) and Fig. 5(d) show the control action u (command acceleration required for the three cameras $C_{c,1}$, $C_{c,2}$, and $C_{c,3}$) for both control laws. At the initial stage of the guidance, a maximum acceleration effort is required for both control laws. However, the control

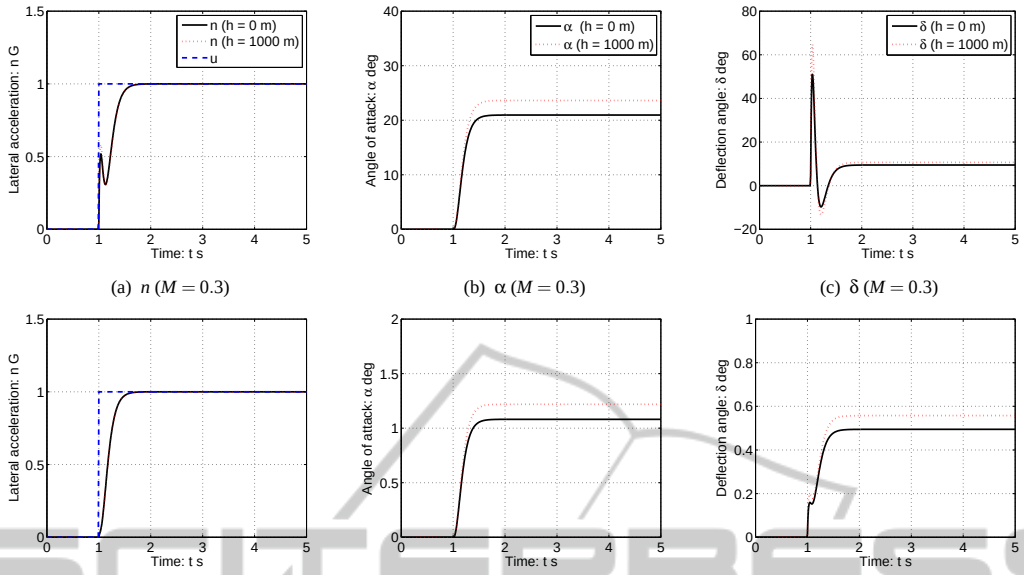

(a) n ($M = 0.3$) (b) α ($M = 0.3$) (c) δ ($M = 0.3$)

(d) n ($M = 0.9$) (e) α ($M = 0.9$) (f) δ ($M = 0.9$)

Figure 3: Autopilot response to step acceleration $u = u_s(t-1)$ G (blue dashed lines) at altitudes $h = 0$ m (black continuous lines) and $h = 1000$ m (red dotted lines). The first and second rows show the outputs for the Mach numbers $M = 0.3$ and $M = 0.9$, respectively.

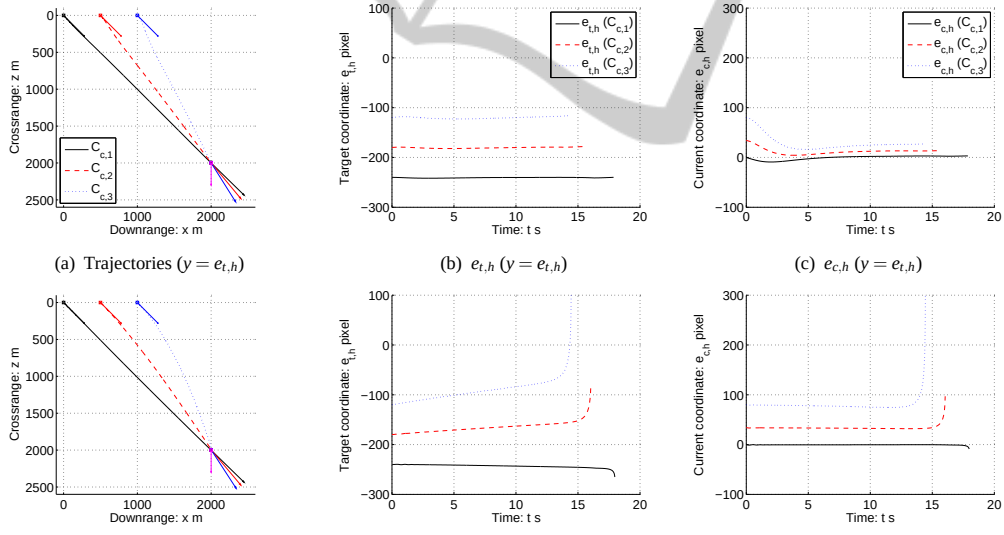

(a) Trajectories ($y = e_{t,h}$) (b) $e_{t,h}$ ($y = e_{t,h}$) (c) $e_{c,h}$ ($y = e_{t,h}$)

(d) Trajectories ($y = e_{c,h}$) (e) $e_{t,h}$ ($y = e_{c,h}$) (f) $e_{c,h}$ ($y = e_{c,h}$)

Figure 4: Outputs of the guidance based on both output $y = e_{t,h}$ and output $y = e_{c,h}$, for the three current cameras $C_{c,1}$, $C_{c,2}$, and $C_{c,3}$, positioned at different space locations but with the same initial attitude angle $\theta_0 = 45$ deg. The first and second rows show the outputs for $y = e_{t,h}$ and $y = e_{c,h}$, respectively.

law based on the coordinate $e_{c,h}$ requires more acceleration than the control law based on the coordinate $e_{t,h}$. Control based on $e_{t,h}$ does not develop high amplitude oscillations at the initial stage of the guidance, but it needs high values of α and δ. Fig. 5(b) and Fig. 5(e) show the angle of attack α, and Fig. 5(c) and Fig. 5(f) show the deflection angle δ, for both control laws. After the initial stage of the guidance, the values of the angles α and δ required for the control law based on $y = e_{c,h}$ are smaller than the values required for the control law based on $y = e_{t,h}$. The camera $C_{c,3}$ requires the highest values of u, α and δ, due to its initial condition; it is ahead of the other cameras and needs more turning effort.

Next, the outputs $y = e_{t,h}$ and $y = e_{c,h}$, are forced to follow an equilibrium reference. Fig. 6(a) and

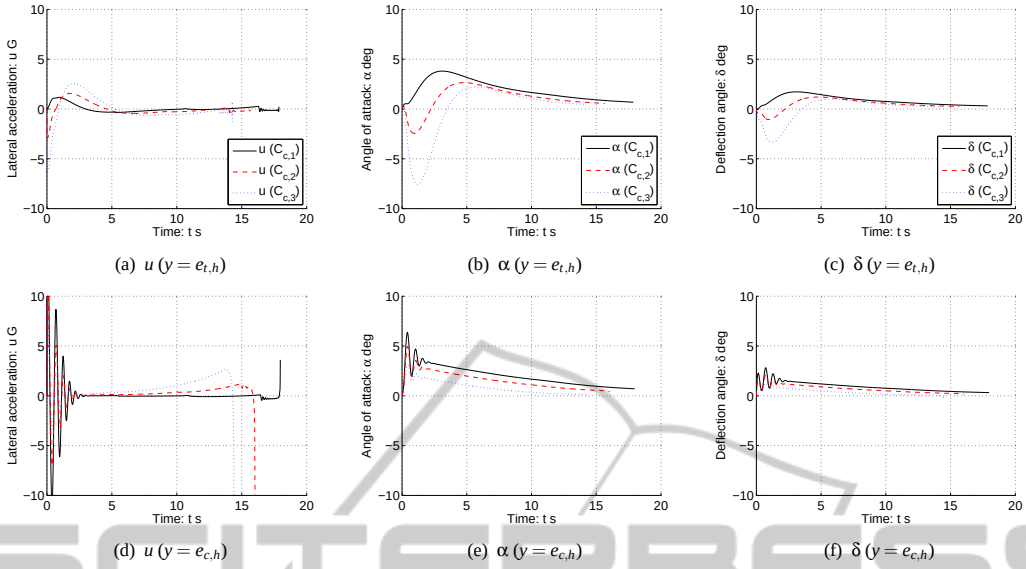

(a) u ($y = e_{t,h}$) (b) α ($y = e_{t,h}$) (c) δ ($y = e_{t,h}$)

(d) u ($y = e_{c,h}$) (e) α ($y = e_{c,h}$) (f) δ ($y = e_{c,h}$)

Figure 5: Acceleration u, angle of attack α, and deflection angle δ for the set of current cameras $C_{c,1}$, $C_{c,2}$, and $C_{c,3}$. The first and the second rows correspond to the controls based on $y = e_{t,h}$ and $y = e_{c,h}$, respectively.

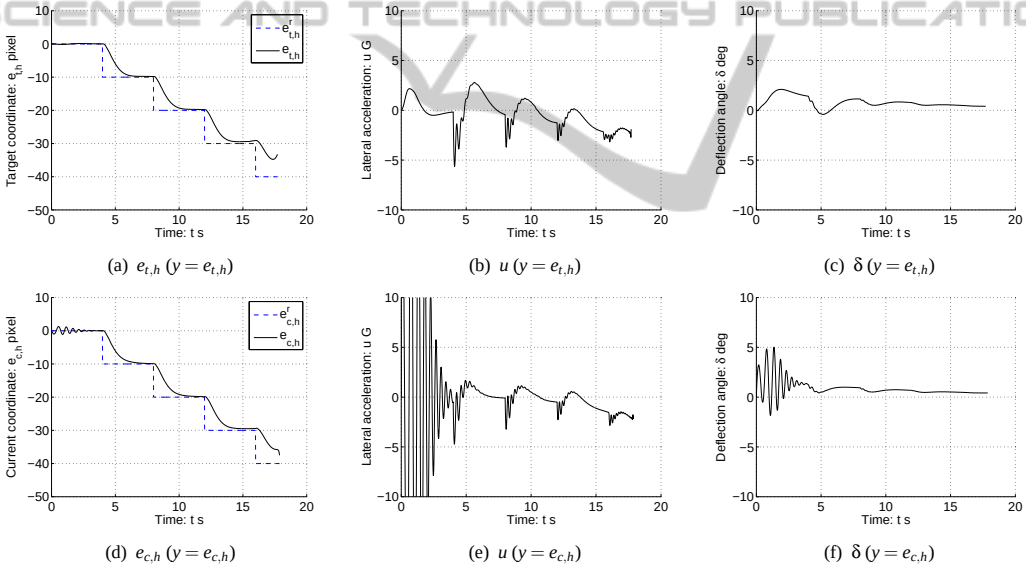

(a) $e_{t,h}$ ($y = e_{t,h}$) (b) u ($y = e_{t,h}$) (c) δ ($y = e_{t,h}$)

(d) $e_{c,h}$ ($y = e_{c,h}$) (e) u ($y = e_{c,h}$) (f) δ ($y = e_{c,h}$)

Figure 6: Outputs for the reference signals $e^r_{t,h} = e^r_{c,h} = -10k$, for $kT \leq t < (k+1)T$, $k = 0,1,2,\ldots$, $T = 4$ s, and $t \geq 0$; acceleration u; and deflection angle δ. The target camera C_t is located at $\mathbf{p}_t = [2000, 2000]^T$ m and aligned to the current camera C_c ($\gamma_t = 45$ deg). The first and second rows correspond to the controls based on $y = e_{t,h}$ and $y = e_{c,h}$, respectively.

Fig. 6(b) show the outputs of the control laws based on $y = e_{t,h}$ and $y = e_{c,h}$ for the reference signals $e^r_{t,h} = e^r_{c,h} = -10k$ pixel, for $kT \leq t < (k+1)T$, $k = 0,1,2,\ldots$, $T = 4$ s, and $t \geq 0$. The initial current camera C_c is located at $\mathbf{p}_c = [0,0]^T$ m with initial attitude angle $\theta_0 = 45$ deg. The target camera C_t is fixed at $\mathbf{p}_t = [2000, 2000]^T$ m and aligned to C_c with attitude angle $\gamma_t = 45$ deg. The gain $\mathbf{K}$ has the same value for both control laws. It is noted that the epipolar coordinates follow the equilibrium references for both control laws. As in the previous simulation, it can be noticed at the initial stage of the guidance, that the control law based on $y = e_{c,h}$ requires more acceleration effort than the other. After this stage, small values of α (Fig. 6(b) and Fig. 6(e)) and δ (Fig. 6(c) and Fig. 6(f)) are required for the control law based on $y = e_{c,h}$. As both outputs can follow the reference, it allows the control laws to guide the vehicle with a reference LoS angle λ to the target position. The angle λ is directly related to the epipolar references

and a limited control of attitude can be achieved by both control laws. In addition, a reduction of the autopilot's gain margin (stability) is noted and the total damping and the time response are affected (see the settling time in the Fig. 6(a) and the Fig. 6(b)). For this simulation the autopilot's design parameters and the control law gain $\mathbf{K}$ were: $\omega_{CR} = 10$ rad/s, $\zeta = 0.7$, $\tau = 0.2$ s, and $\mathbf{K} = [8,2,8]$. Moreover, the initial stage of the guidance is the worse flight condition that the autopilot has to deal with. For high altitude h and low Mach number M, the autopilot requires the higher values of α and δ. This initial condition affects more the control law based on $y = e_{c,h}$ than the control based on $y = e_{t,h}$. One way to improve the initial response of the autopilot is to rise the value of the vehicle's initial velocity, but it will always be constrained.

6 CONCLUSIONS

An epipole-based control law for guiding an autonomous UAV has been presented. Only epipolar measurements from two views were used to drive the vehicle to a static camera position. Stabilization of a nonlinear engagement rule by an input-output nonlinear control strategy was developed and two different alternatives for guidance, one based on the current epipolar coordinate, and the other based on the target epipolar coordinate, were studied. A state feedback control law with integral action guaranteed that the epipolar coordinates follow a reference equilibrium signal. A model of a non-propelled UAV, that includes a classical three-loop autopilot, was used to simulate the control strategies. The tracking of reference signals and stability analysis will be studied as future developments.

ACKNOWLEDGEMENTS

This work was supported by Universidad de los Andes / Industria Militar de Colombia (INDUMIL), Universidad de Zaragoza / Ministerio de Ciencia e Innovación / Unión Europea DPI2009-08126, and Universidad de Nariño.

REFERENCES

Chin, S. (1961). *Missile configuration design*. McGraw-Hill, 1st edition.

Hartley, R. I. and Zisserman, A. (2004). *Multiple View Geometry in Computer Vision*. Cambridge University Press, ISBN: 0521540518, 2nd edition.

Hu, G., Gans, N., Mehta, S., and Dixon, W. (2007a). Daisy chaining based visual servo control part ii: Extensions, applications and open problems. In *IEEE International Conference on Control Applications, 2007*, pages 729 – 734.

Hu, G., Mehta, S., Gans, N., and Dixon, W. (2007b). Daisy chaining based visual servo control part i: Adaptive quaternion-based tracking control. In *IEEE International Conference on Control Applications, 2007*, pages 1474 – 1479.

Kaiser, M. K., Gans, N. R., and Dixon, W. E. (2010). Vision-based estimation for guidance, navigation, and control of an aerial vehicle. *Aerospace and Electronic Systems, IEEE Transactions on*, 46(3):1064 – 1077.

Khalil, H. K. (2002). *Nonlinear Systems*. Prentice Hall, ISBN: 0130673897, 3rd edition.

López-Nicolás, G., Guerrero, J., and Sagüés, C. (2010). Visual control of vehicles using two-view geometry. *Mechatronics*, 20(2):315 – 325.

López-Nicolás, G., Sagüés, C., Guerrero, J., Kragic, D., and Jensfelt, P. (2008). Switching visual control based on epipoles for mobile robots. *Robotics and Autonomous Systems*, 56(7):592 – 603.

Ma, L., Cao, C., Hovakimyan, N., and Woolsey, C. (2007). Development of a vision-based guidance law for tracking a moving target. In *AIAA Guidance, Navigation and Control Conference and Exhibit*. AIAA.

Mariottini, G., Prattichizzo, D., and Oriolo, G. (2004). Epipole-based visual servoing for nonholonomic mobile robots. In *IEEE International Conference on Robotics and Automation, 2004*, volume 1, pages 497 – 503.

Melin, T. (2000). A vortex lattice matlab implementation for linear aerodynamic wing applications. Master's thesis, Royal Institute of Technology (KTH).

Schneiderman, R. (2012). Unmanned drones are flying high in the military/aerospace sector [special reports]. *Signal Processing Magazine, IEEE*, 29(1):8 – 11.

Siouris, G. M. (2004). *Missile Guidance and Control Systems*. Springer New York, ISBN: 9780387007267, 1st edition.

Watanabe, Y., Johnson, E., and Calise, A. (2006). Vision-based guidance design from sensor trajectory optimization. In *AIAA Guidance, Navigation and Control Conference and Exhibit*. AIAA.

Yanushevsky, R. (2007). *Modern Missile Guidance*. CRC Press, ISBN: 1420062263, 1st edition.

Zarchan, P. (2007). *Tactical and Strategic Missile Guidance*. American Institute of Aeronautics and Astronautics Inc., ISBN: 9781563478741, 5th edition.